Picosecond Photoluminescence Study of the *n*-GaAs(100)/Methanol Interface in a Photoelectrochemical Cell

T. A. Abshere and G. L. Richmond*

Department of Chemistry and Materials Science Institute, University of Oregon, Eugene, Oregon 97403

Received: May 3, 1999; In Final Form: July 13, 1999

Anodic photocorrosion and cathodic photowashing of *n*-GaAs(100) in a nonaqueous photoelectrochemical cell have been studied using photoluminescence decays and the voltage dependence of both photoluminescence intensity and photocurrent. Photocorrosion of the cell, which is attributed to trace water contamination, results in an increased surface recombination velocity and an overall loss in photoluminescence intensity, but does not affect the photocurrent. The stability of the photocurrent upon corrosion of the cell implies that the photoinduced surface states resulting from the corrosion are intrinsically different from those observed in all other systems studied previously in this laboratory. The techniques listed above were also used to monitor changes in the *n*-GaAs/methanol interface with incremental water additions to the cell to study the effects of water contamination.

I. Introduction

For several decades, semiconductor/electrolyte photoelectrochemical cells (PEC) have been studied as an alternative to standard solid-state solar energy converters. However, the use of *n*-doped semiconductors such as *n*-GaAs has been hampered by anodic photocorrosion of the semiconductor surface, limiting the efficiency and effective lifetime of potential devices. Previous work in this laboratory focused on *n*-GaAs aqueous liquid junction cells and gaining a better understanding of the chemistry and interfacial properties that affect processes such as charge transfer, corrosion, and passivation in these cells. The current study is a move into the nonaqueous regime to further our understanding of the properties of *n*-GaAs.

Three factors influenced the decision to study the *n*-GaAs/electrolyte interface using methanol as the solvent. First, water has been shown to play an important role in both corrosion and passivation processes.[1−4] Moving into the nonaqueous regime offers the opportunity to control corrosion and study unmediated charge transfer from the semiconductor to the redox species. The effect of water contamination in the methanol cells can be monitored by spiking the cell with small water additions. Second, there are a variety of outer-sphere redox couples available that are stable in methanol[5] with equilibrium potentials within the band gap of *n*-GaAs. The ferrocene/ferricenium couple was chosen for this study because its equilibrium potential is close to the *n*-GaAs valence band edge and because of the extent of information available on it in the literature. Finally, the use of a redox couple other than sodium sulfide (used extensively in previous *n*-GaAs studies from this and other laboratories)[6−10] raises the possibility of utilizing a passivating layer on the *n*-GaAs surface as a controllable parameter.

In the studies described here we examine the *n*-GaAs/methanol interface using picosecond photoinduced luminescence. Two types of measurements have been conducted. The first consists of time-resolved photoluminescence (TRPL) measurements. TRPL decays are used to indicate changes in the surface recombination velocity (SRV) resulting from anodic corrosion or other processes that affect the density of trap states at the interface. This relationship is indicated in the following equation:

$$S = \sigma \nu_{th} N_t \tag{1}$$

where S is the surface recombination velocity, σ is a trapping cross section, ν_{th} is the minority carrier thermal velocity, and N_t is the number of surface traps per unit area—including both intrinsic surface states (ISS) and photoinduced surface states (PSS).[11] The second examines photoluminescence and photocurrent as a function of applied potential. These studies give information on the location of PSS and whether those states affect charge transfer across the interface.

The power dependence of the decays indicates that, at the laser powers used here, the illumination is sufficient to saturate the ISS at the interface. ISS are states within the band gap of the bulk GaAs that exist at the surface due to the imperfect termination of the semiconductor crystal lattice. The density and location of ISS are dependent on the solvent used, the exposed crystal face (indicated in this work by Miller indices), and the presence of adsorbed species or an oxide layer.[1,12,13] Saturating the ISS is necessary to populate otherwise inaccessible higher energy PSS created in photocorrosion events.[14,15] Anodic photocorrosion is a buildup of PSS due to oxidation of the *n*-GaAs surface. The PSS act as an additional nonradiative recombination path, which reduces overall photoluminescence yield and may interfere with charge transfer across the interface. Signs of photocorrosion include a drop in photoluminescence intensity at potentials that access the PSS, an increase in decay rate, an increase in SRV, decreased cell efficiency, and (often) a decrease in photocurrent.[11,16−18]

An important aspect of these studies is the comparison of the *n*-GaAs/methanol properties with those measured with similar methods on *n*-GaAs/aqueous systems. Unless specifically noted, all comparisons with the aqueous work performed previously in this laboratory refer to *n*-GaAs(100) in cells containing 0.25 M $Na_2S{\cdot}9H_2O$ as the redox salt. The aqueous cells suffer anodic photocorrosion, resulting in an increase in the measured SRV and a loss of photocurrent. The sulfide passivates *n*-GaAs for a limited period of time. Low concentra-

10.1021/jp991443w CCC: $18.00
Published on Web 08/27/1999

tions of Na_2S (0.25 M) allow the cell to corrode rapidly, producing a density of PSS detectable in the optical studies as a dip in PL signal in the depletion region of photoluminescence versus voltage (PL−*V*) scans. High Na_2S concentrations (2 M) slow corrosion but eventually lead to a buildup of PSS across the entire band gap.[17] The drop in PL from photocorrosion is visible in PL−*V* scans only when the light intensity and laser repetition rate are high enough to saturate the ISS at the interface.

One of the most important results of this study is that the *n*-GaAs/methanol cells also undergo anodic photocorrosion. Exposing the cell to light under depletion conditions results in measurable increases in the SRV as seen from modeling TRPL decays. PL−*V* scans show that when corrosion occurs in these cells, it produces a distribution of photoinduced states, which spans the band gap. Current−voltage curves (*I*−*V*) taken simultaneously with the PL−*V* scans show that the photoinduced surface traps do not appear to affect charge transfer across the interface. The photocurrent remains the same even after corrosion is clearly evident in both TRPL decays and PL−*V* scans. In addition, both the PL−*V* and the *I*−*V* data show interesting changes when water is incrementally added to the cell.

II. Experimental Considerations

The experiments were performed on *n*-GaAs(100) crystal wafers [Crystal Specialties] with a (Si-doped) carrier concentration of $(2-4) \times 10^{17}$ cm^{-3}. The back of the *n*-GaAs was etched for 2 min with a solution of 2:1:1 H_2SO_4 (96.7%)/H_2O/H_2O_2 (30%) and then placed in contact with a copper electrode using an indium/gallium eutectic. The front surface of the *n*-GaAs was etched (0.05% Br_2/MeOH solution for 15 s followed by 1 M KOH for 30 s, and repeated at least three times) before the sample was introduced into a drybox where the rest of the electrochemical cell and the dried chemicals were held. The cells were put together inside the drybox, which generally contained <0.2 ppm O_2, and were sealed before being brought out and placed in front of the laser. All chemicals other than ferricenium and $LiClO_4$ were obtained from Aldrich. Anhydrous methanol (<0.002% H_2O) was purified by distilling over sodium followed by three freeze−pump−thaws to degas before introduction to the drybox. $LiClO_4$ was obtained from Alfa Aesar and dried by heating under vacuum for several days. Ferrocene was used as received. Ferricenium was oxidized electrochemically from ferrocene in the presence of $LiClO_4$ to give the ferricenium perchlorate salt, which was dried under vacuum. Unless specifically noted in the paper, the nonaqueous cells contained 0.7 M $LiClO_4$/0.02 M $FeCp_2$/0.005 M $FeCp_2^+ClO_4^-$ in 50 mL of methanol. Comparisons with aqueous cells studied previously in this lab refer to *n*-GaAs(100) in cells containing 0.25 M $Na_2S{\cdot}9H_2O$ as the redox salt unless otherwise noted.

For all experiments, the cells were held under potentiostatic control in a three-electrode configuration. The counter electrode (CE) was a platinum wire. The reference electrode (RE) was either a platinum wire poised at the electrolyte equilibrium potential or a Ag/(0.01 M)$AgNO_3$ nonaqueous reference (from BAS) in a 0.7 M $LiClO_4$ methanol solution separated from the main cell by a vicore frit. The $Ag/AgNO_3$ electrode was measured to be 0.46 V vs saturated calomel electrode. The equilibrium cell potential (Pt vs $Ag/AgNO_3$) was measured to be −0.31 V. All potentials in the paper are scaled to the $Ag/AgNO_3$ reference electrode for clarity. The working electrode typically had a dark open circuit voltage (V_{oc}) of −0.42 V vs $Ag/AgNO_3$ immediately after introduction to the cell. According to work by B. Ba et al.,[5] the flat band potential (V_{fb}) for the *n*-GaAs/methanol cell is −1.5 V vs $Ag/AgNO_3$. V_{fb} was verified by Mott−Schottky analysis. The working electrode was placed within 1 cm of the optical window to minimize any absorption effects of the electrolyte on either the laser light or the band gap luminescence.

All of the experiments in this paper were performed either without any applied potential or within the potential range from flat band potential ($V_{fb} = -1.5$ V) to deep depletion. When no potential is applied, the cell is at the open circuit potential (V_{oc}) which varies depending on illumination. All investigated potentials more positive (less negative) than V_{fb} are in the depletion regime where a space charge layer exists in the semiconductor near the interface. A significant amount of work was performed with the cell held at 0.0 V, which will be referred to as V_{dep} throughout the rest of the paper.

For the photoluminescence studies, the *n*-GaAs is illuminated at near normal incidence by the pulse-compressed (∼5 ps) frequency-doubled (to 532 nm) output of a mode-locked Nd:YAG laser. Details of the laser system have been described elsewhere.[14,15] Selecting pulses with an acoustooptic modulator controls the repetition rate with an extinction coefficient in excess of 200:1. Power is adjusted with a half-wave plate/polarizer. Band gap luminescence (855 nm) is filtered with a 610 nm long-pass filter and monochromator before being collected by a cooled microchannel plate PMT feeding a 1.8 GHz amplifier attached to a constant-fraction discriminator. The TRPL decays are taken with a time correlated single-photon counting technique[19] using the discriminator as a start pulse and a fast photodiode—detecting a portion of the pulse separated prior to illuminating the sample—as the stop pulse. The microchannel plate has a time resolution of 11.1 ps; however, system response functions (obtained by measuring scattered 532 nm light) have a full width half-maximum of approximately 80 ps. For qualitative comparisons the decays are viewed as measured. When the decays are modeled to determine the SRV, the system response function is first deconvolved from the measured decays.

The spot size illuminating the *n*-GaAs was characterized by knife-edge measurements independently across the vertical (ω_v) and horizontal (ω_h) transverse profiles of the beam. The beam is elliptical at the sample—most likely a result of the use of the AOM for eliminating pulses earlier in the beam path. Assuming an approximately Gaussian transverse spatial profile, the distance between knife-edge positions passing 16% and 84% of the total beam energy was used to approximate the Gaussian beam radius ω, which is the half-width at $1/e$ of the maximum for field amplitude, or $1/e^2$ of the maximum for intensity.[20] The Gaussian beam radius ω is related to the fwhm for the intensity by fwhm $= (2Ln2)^{1/2}\omega$. The area of the spot used for measuring photon flux (photons/cm^2·pulse) was taken to be $\pi\omega_v\omega_h = 1.70 \times 10^{-4}$ cm^2 where $\omega_v = 60$ μm and $\omega_h = 90$ μm.

The SRV is obtained by modeling the TRPL decays with the equation

$$I(t)/I(0) = [(1/A)\exp(A^2T)\,\mathrm{erfc}(AT^{1/2}) - (1/S)\exp(S^2T)\,\mathrm{erfc}(ST^{1/2})][SA/(S-A)]\exp(-T) \quad (2)$$

where $I(t)$ is the PL intensity at time t and A, T, and S are the reduced absorption coefficient ($\alpha(D\tau)^{1/2}$), reduced time (t/τ), and reduced SRV ($s(\tau/D)^{1/2}$), respectively. α is the absorption coefficient (calculated to be 78 421 cm^{-1} from measured values of the complex refractive index),[21] τ is the bulk luminescence lifetime (6.4 ns from the van Roosbroeck−Shockley value),[22] s is the SRV, and D is the ambipolar diffusion coefficient (5.5

cm^2/s based on the doping density of the samples).[23] Equation 2 is derived from the 1-D continuity equation for the minority carriers assuming a semi-infinite semiconductor slab after excitation with a δ function light pulse. The semiconductor used in this work is doped *n*-type so a solution to only the minority carrier continuity equation is adequate to model the TRPL decays. If the semiconductor was only intrinsically doped and the light pulses significantly perturbed the concentration of both charged species, then the ambipolar equation may have been a more appropriate choice for modeling the decays.

As in the aqueous studies,[24] eq 2 is modified to treat the SRV as a parameter that changes with time to reflect trap saturation and the resultant change in the activation energy of trap occupation. The SRV used in the above equation becomes

$$s(t) = s_o \exp[-V((1 - \exp(-t/\tau_c))/k_b T_k)] \qquad (3)$$

where s_o is the initial SRV, V is the trap barrier height at long times, τ_c is a time constant characterizing the evolution of the trap barrier height following laser pulse illumination, k_b is the Boltzmann constant, and T_k is the temperature. The time evolution of the ambipolar diffusion coefficient is not considered a dominant factor in the observed decays. If it was, it would lead to longer decays with lower excitation power densities, which is opposite the trend we observe. In performing the simulations, we chose the initial SRV such that the early portion of the decay was reproduced without the inclusion of the time-dependent trap barrier. The experimental decays were then simulated by adjusting V and τ_c. The cumulative uncertainty in the simulation precludes stating the precision of the measurements to better than a factor of 2−3. The stated precision (±5%) reflects the sensitivity of the fit to only the SRV, all other uncertainties held equal.

III. Results and Discussion

A. Time-Resolved Photoluminescence Decays. The rate of decay of the PL signal (and also the SRV) after excitation of the semiconductor by a picosecond laser pulse is sensitive to the density of surface states at the interface. Photocorrosion in the cell is studied by monitoring PSS as manifested by changes in the TRPL decay rate. Creation of PSS increases the SRV (eq 1), giving a faster photoluminescence decay (eq 2). As stated previously, PSS are accessed only when the interface is illuminated with sufficient light intensity to saturate the ISS. When the intensity is too low to saturate the ISS, the SRV is effectively infinite, screening by accumulated charge carriers is not observed, and an increase in the number of surface traps is not expected to affect the PL intensity.[11] To ensure that the TRPL decays are sensitive to interfacial processes that affect the density of surface states in the methanol-containing cells, the present investigation was performed in a laser intensity regime where the intrinsic traps were saturated. To show this, TRPL decays were taken at several light intensities. All decays were taken at the flat band potential (−1.5 V) to minimize space charge field effects, making the measurement sensitive to the intrinsic SRV.

Figure 1 shows that, as the photon flux is increased from (c) to (a), the decay rate and observed SRV decrease. The change in observed SRV resulting in slower decays at lower incident flux indicates that the intrinsic traps are saturated, giving finite values for the observed SRV. Photon fluxes higher than those used in Figure 1a (1.62×10^{13} photons/cm^2·pulse) resulted in only a small change in the rate of decay. Further corroboration for the assertion that the system is in a saturated surface state

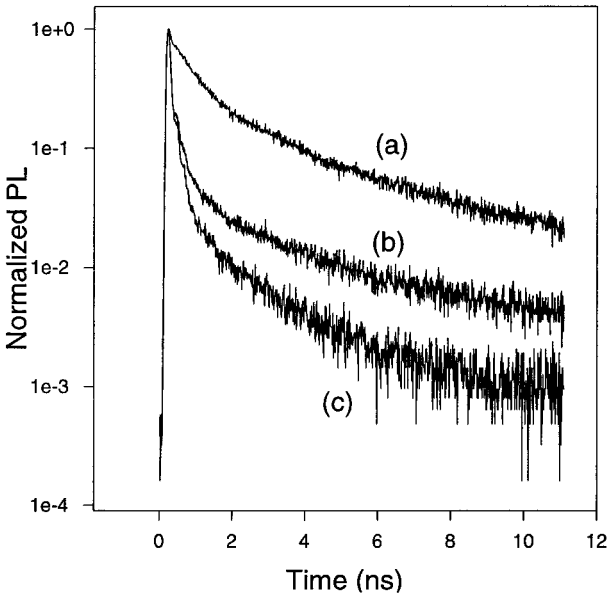

Figure 1. Photoluminescence decays at V_{fb} (−1.5 V) with a 951 kHz laser repetition rate and with photon fluxes of (a) 1.6×10^{13} photons/cm^2·pulse, (b) 1.6×10^{12} photons/cm^2·pulse, and (c) 1.6×10^{11} photons/cm^2·pulse.

regime was obtained when the decays were modeled. Modeling these decays with eq 2 requires the use of the modified SRV, which takes into account time-dependent trap saturation and the change in trap occupation with activation energy.[24] If the cell is in a regime where the traps are not saturated, the SRV is effectively infinite and the decays can be modeled without the time-dependent parameters introduced in eq 3.

Figure 2 shows the results of exposing the cell to high-intensity light (1.62×10^{13} photons/cm^2·pulse at 951 kHz) while the cell was held at different potentials. For each figure, two traces were recorded with the trace labeled "fresh" corresponding to a sample with a freshly etched *n*-GaAs surface and the trace labeled "exposed" corresponding to a sample after the *n*-GaAs was exposed to laser light under the conditions described below.

Exposing the cell to light while in deep depletion (V_{dep}) results in photocorrosion as indicated by an increase in the SRV after exposure. With respect to the corrosion studies, V_{dep} will always refer to 0.0 V vs $Ag/AgNO_3$ specifically. Decays taken at potentials ranging from V_{dep} (2a) to V_{fb} (2b) all show a marked increase in both SRV and decay rate after V_{dep} light exposure. We attribute the increase in SRV after V_{dep} light exposure to the creation of PSS, which act as an additional nonradiative recombination path for electrons and holes at the interface. The PSS span the entire *n*-GaAs band gap, resulting in increases in decay rates at a variety of potentials, although only the extremes of the investigated potential range are presented to conserve space. Possible sources for the photocorrosion that leads to PSS will be addressed later.

Figure 2c shows decays taken at V_{fb} before and after the cell was illuminated for several minutes at V_{fb}. Unlike the results at depletion potentials, extended exposure of the cell to light at V_{fb} does not result in photocorrosion. The decay taken after illumination has a slower decay rate (and smaller SRV) than the fresh surface. We attribute the smaller SRV to photowashing; i.e., ISS are being removed from the interface. The term photowashing is used in this context to describe any process that removes surface states. Photowashing results in enhanced saturation of the remaining surface states by the laser pulses and a decrease in the observed SRV. Possible causes of

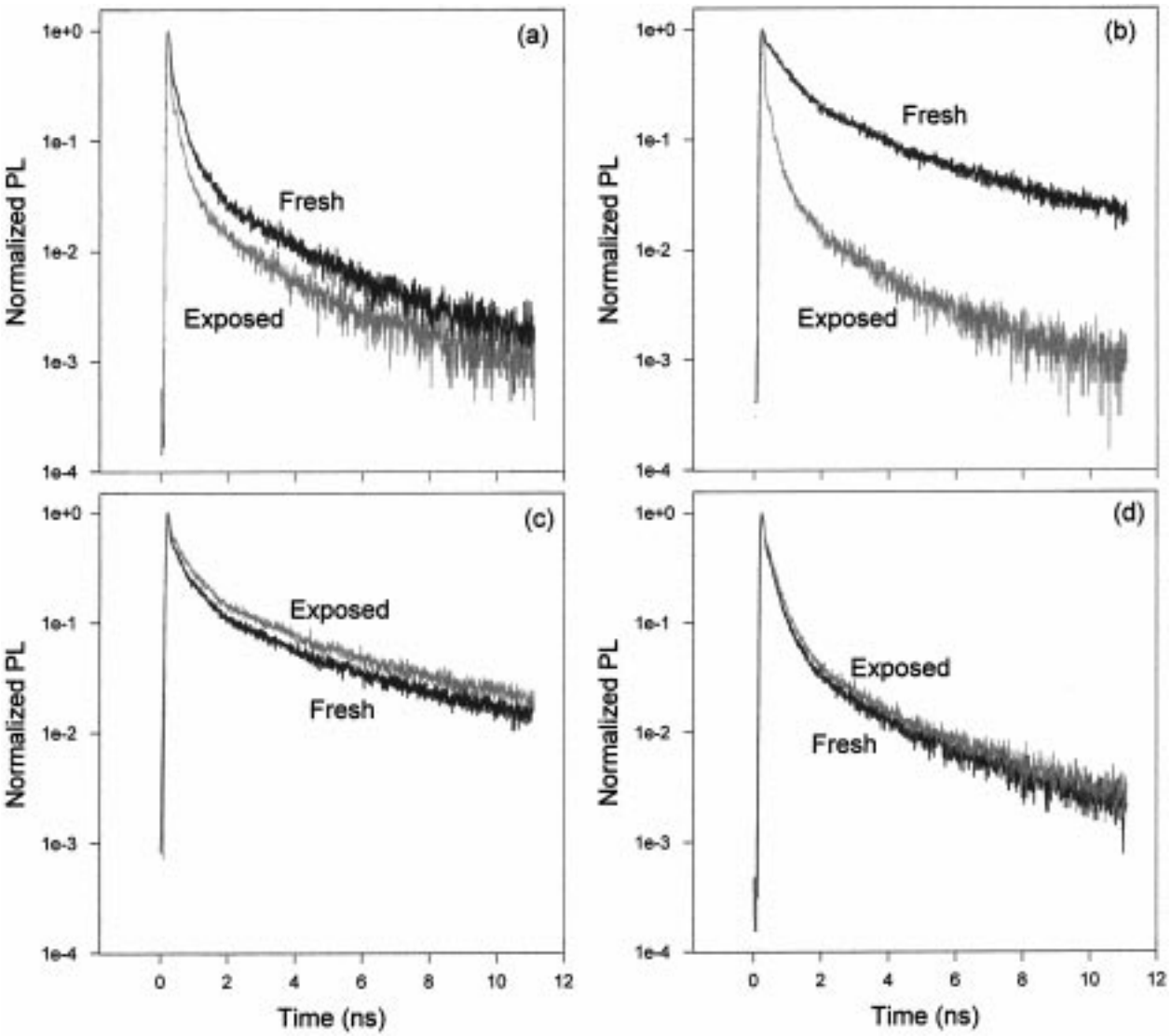

Figure 2. PL decays before and after light exposure at a 951 kHz laser repetition rate and with a photon flux of 1.6×10^{13} photons/cm^2·pulse under the following applied potentials: (a) light exposure at V_{dep} (0.0 V), decays taken at V_{dep}; (b) exposure at V_{dep}, decays taken at V_{fb} (−1.5 V); (c) exposure at V_{fb}, decays taken at V_{fb}; (d) exposure at V_{oc}, decays taken at V_{oc}. Figure 2b also shows the modeled fit used to determine the "before corrosion" SRV value in Table 1.

photowashing include the removal of an oxide layer, removal of other adsorbed species,[25] or the loss of surface states that were caused by defect sites on the surface.[18]

With the information currently available, it is difficult to determine whether the photowashing involves a structural change of the *n*-GaAs surface or a removal of adsorbed contaminants/oxides from the *n*-GaAs surface. Whatever the cause, the photowashing does not reverse the effects of any photocorrosion caused by previous V_{dep} exposure. In addition to photowashing with V_{fb} light exposure, there are other factors that could be contributing to the observations at V_{fb}.

First, the *n*-GaAs is capable of reducing methanol electrochemically at this potential. This may be affecting the chemistry occurring at the interface, for example, by mediating charge transfer of the majority carrier into solution.

Second, the TRPL decays are not reproducible at V_{fb} without first preparing the interface by sweeping the potential to V_{dep} and back under illumination. Sweeping the potential in this way increases the photoluminescence being collected at V_{fb} by a factor of 2−3 as compared to the photoluminescence from the same spot on the sample before the potential sweep (the shutters on the PMT are always readjusted before the TRPL decay is collected to reduce the collected photoluminescence to approximately 2000 counts/s to avoid pulse pileup). We also attribute the increase in photoluminescence during the preparatory sweep to photowashing. Although the TRPL decays taken without the sweep are not reproducible, they always have a faster decay rate than TRPL decays taken after a preparatory sweep. The decays labeled "fresh" in Figure 2 were all taken after the potential was swept as described above. The decreased decay rate visible in the decay labeled "exposed" in Figure 2c shows additional photowashing with continued light exposure at V_{fb}.

Figure 2d shows decays measured at open circuit voltage (V_{oc}) before and after significant illumination at V_{oc}. The PEC is not held under potentiostatic control during these measurements, simulating the desired working conditions for photoelectrochemical solar energy converters.[26] V_{oc} was typically measured at approximately −0.83 V at the start of a TRPL scan and −0.61 V by the end of the scan with a total collection time of 200 s. There is little change in the (exposed) decay measured after V_{oc} light exposure as compared to the (fresh) decay, and we conclude that under these conditions the cell does not corrode. For the corrosion seen in Figure 2a,b to occur, we have to apply a potential to the cell to force it into an anodic configuration.

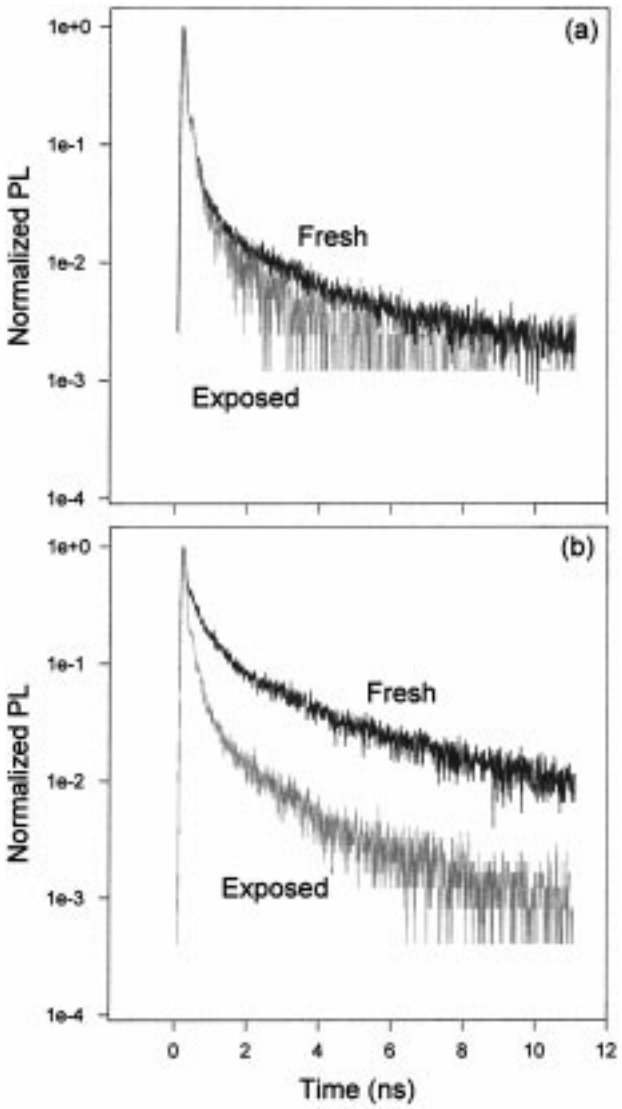

Figure 3. PL decays before and after V_{dep} (0.0 V) light exposure at a 951 kHz laser repetition rate with photon fluxes of 1.6×10^{13} photons/cm^2·pulse. Decays are shown for the following conditions: (a) decays of fresh and exposed surfaces with a 951 kHz repetition rate and 8.1×10^{11} photons/cm^2·pulse; (b) decays of fresh and exposed surfaces with a 238 kHz repetition rate and 8.1×10^{12} photons/cm^2·pulse.

The ability to observe changes in the SRV from TRPL decays at the flat band potential has been investigated as a function of power level and repetition rate of the laser pulses. Corrosion induced in a sample (in depletion with high laser power) is observable at a variety of power levels and repetition rates as long as intrinsic trap saturation conditions are met. As stated previously, the ISS must be saturated before the higher energy PSS created by photocorrosion are accessed. Figure 3a shows that at low photon flux (8.12×10^{11} photons/cm^2·pulse) the effects of cell corrosion can just barely be seen in the decays, indicating that the laser intensity is just above the trap saturation level. Below this level, we conclude that the SRV is effectively infinite and the decays are insensitive to creation of PSS.

The repetition rate has previously been used as a variable parameter to estimate the PSS emptying/refilling time. In the aqueous sodium sulfide cells, corrosion effects were observed in PL−*V* scans taken at 951 kHz but not at 238 kHz.[11] This placed the lifetime of trap occupation by holes between 1 μs (1/951 kHz) and 4 μs (1/238 kHz). Figure 3b shows TRPL decays from an *n*-GaAs/methanol cell taken at 238 kHz from corroded and fresh spots on the sample. The photon flux for these scans was reduced to 8.12×10^{12} photons/cm^2·pulse in case the intrinsic trap states are saturated by individual laser pulses at the higher photon flux normally used. It is obvious from the decays that, in the methanol cell, the traps are still saturated at 238 kHz. This suggests that the trap occupation lifetime in the methanol cell is longer than the 4 μs maximum lifetime estimated for the aqueous cells.

TABLE 1:

cell	SRV ($\pm 0.05 \times 10^5$ cm/s)	V (eV)	T_c (ns)
before corrosion	1.35	0.056	1.4
after corrosion	>5	0.051	1.1
H_2O added	4.50	0.054	1.4
aqueous Cell	1.13		

The results obtained from modeling the TRPL decays are summarized in Table 1. The three parameters varied in the model are the SRV, the V (eV)—trap barrier height at long times—and the T_c (ns)—time constant characterizing the evolution of the trap barrier height. The corrosion results refer to decays after exposure of the cell to illumination in depletion conditions, which results in a decrease in overall photoluminescence and an increase in the decay rate. The photon flux and repetition rate are the same for all nonaqueous cell decays, 1.62×10^{13} photons/cm^2·pulse and 951 kHz, respectively. The cell with water added contained enough water to eliminate the voltage dependence of the photoluminescence (see discussion below). The aqueous cell contained 0.25 M Na_2S.[18] All of the decays in the table were taken at flat band potential as determined for each individual cell. The freshly etched methanol-containing cells start out with a SRV slightly higher than the aqueous cell. With either corrosion or water addition, the SRV increases dramatically, indicating significant changes occurring at the interface.

B. Photoluminescence versus Voltage. PL−*V* scans give useful information for determining the location of PSS within the band gap. Figure 4a shows data corresponding to a drop in PL after multiple sweeps of the applied potential between V_{fb} and V_{dep}. Scan (i) in Figure 4a is the first sweep of the potential from V_{fb} to V_{dep}. Scan (ii) is a later sweep (the 11th full sweep) in the same range, showing a drop in PL across the entire potential range. We attribute the drop in PL at all applied potentials within the investigated range to a distribution of surface states spanning the band gap. This agrees with the TRPL decay results showing corrosion at a variety of applied potentials (Figure 2a,b). If PSS build up in a localized region of the band gap[11]—such as in the aqueous cells with low Na_2S concentrations—they show up in a PL−*V* scan as a drop in photoluminescence only in the potential window that allows these states to be accessed. Buildup of PSS over a wide potential range as seen here results in a drop in PL across the entire band gap.

Scan (iii) in Figure 4a shows the PL−*V* after water is added to the cell (1:50 water/methanol). The PL completely loses any voltage dependence after this much water is added. The TRPL decays in Figure 4b corroborate the lack of voltage dependence by showing that there is no difference in decays taken from V_{fb} to V_{dep}. The results from smaller water additions will be examined in the next section. One explanation for the loss of voltage dependence is that the *n*-GaAs/mixed solvent interface has an increased density of intrinsic surface states over the *n*-GaAs/methanol system. The surface states are no longer saturated by the laser illumination, and the decays are therefore no longer sensitive to changes in the interface. However, simply dropping below trap saturation levels is not sufficient to explain the complete loss of potential dependence of the PL. According

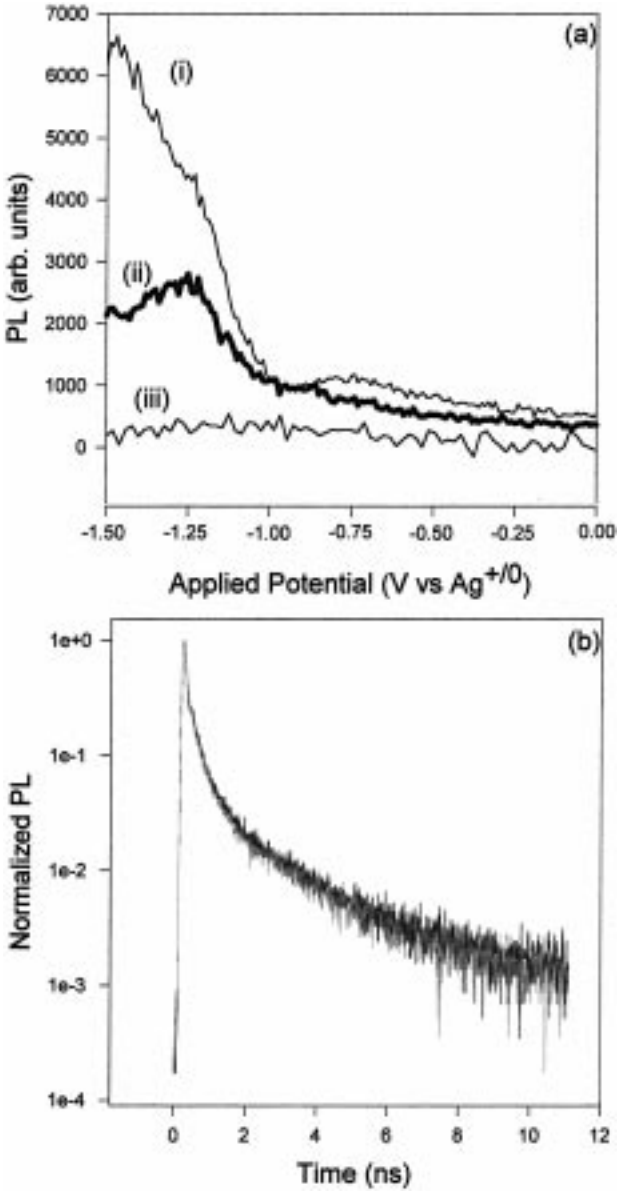

Figure 4. (a) PL−*V* scans for (i) a fresh sample, (ii) a sample corroded by cycling the voltage many times with light exposure, and (iii) a sample after the cell was spiked with water. Note: the PL scale for (i) and (ii) is the same so they can be compared directly; (iii) was lowered slightly on the PL scale to reduce clutter in the figure. (b) PL decays at V_{fb} and V_{dep} after the water addition.

to the dead layer model, which was used to model PL−*V* behavior in the aqueous cells,[15] below trap saturation levels the relationship between PL and applied potential is as follows:

$$I_{pl} = I^{\infty} \exp(-\alpha W) \qquad (4)$$

where I_{pl} is the measured luminescence intensity, I^{∞} is the luminescence at V_{fb} assuming infinite SRV, α is the absorption coefficient, and W is the width of the depletion layer in the semiconductor. Since the PL does not follow the form of eq 4, we conclude that the behavior of the cell after water addition cannot be simply attributed to a change in the density of ISS from changing the solvent contents.

The lack of any voltage dependence at all in part a (iii) and b of Figure 4 indicates that the density of states is large enough at the interface to effectively "metallize" the semiconductor.[12] In this case, the applied potential results in a potential drop

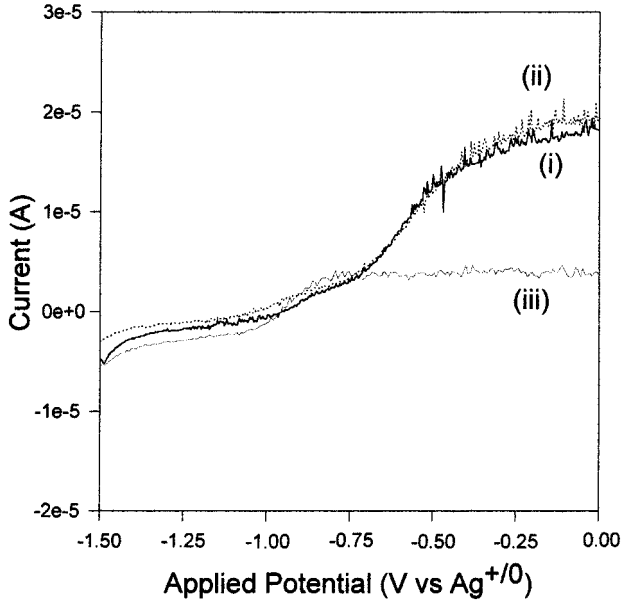

Figure 5. *I*−*V* curves corresponding to the PL−*V* scans in Figure 4: (i) fresh; (ii) corroded; (iii) water added.

predominantly in the Helmholtz region of the electrolyte rather than in the space charge region of the semiconductor. The band bending is then desensitized to the applied potential and the PL remains constant while the potential is swept. Part of the buildup of interface states with water addition likely involves the formation of a film on the surface of the *n*-GaAs. If a thick oxide layer is formed, the *n*-GaAs becomes insulated from the electrolyte and the Fermi level becomes pinned by the large density of *n*-GaAs/oxide interface states,[13] preventing changes in the band bending with applied potential. Future XPS studies will be used to examine this possibility.

C. Current versus Voltage Measurements. Current−voltage curves are often a useful complimentary technique to the optical techniques used to study the semiconductor/liquid interface. In the case where corrosion is induced, photocurrent can be monitored to determine if the PSS are charge-transfer mediators or charge-transfer inhibitors or are not involved in the charge transfer to the redox in solution. Figure 5 shows the *I*−*V* curves recorded simultaneously with the PL−*V* scans in Figure 4a. It is clear from these results that the fresh surface (i) and corroded surface (ii) scans are superimposable. Photocorrosion does not result in a change in the observed photocurrent despite the dramatic drop present in the PL. Thus, we conclude that the PSS are not involved in mediating charge transfer across the interface. Caution must be taken when using photocurrent to monitor PEC corrosion, as this is not the only example of a PEC corroding without a change in photocurrent.[16]

The other *I*−*V* in Figure 5 (iii) is of a methanol cell contaminated with water. This cell shows a significant loss in photocurrent, which is most likely due to one of two causes. First, the surface states created upon water addition are charge-transfer inhibitors and therefore fundamentally different from the corrosion states in the absence of water. Second, a buildup of oxide film on the *n*-GaAs surface prevents charge transfer. The lack of voltage dependence to the PL after water addition rules out a simple change in the density of surface states, which indicates the second choice is the most likely.

Close examination of the oxidation peak (photocurrent) in a typical *I*−*V* curve (Figure 6a) reveals what appears to be two oxidation peaks between −1.0 and 0.0 V. The photocurrent begins increasing at approximately −1.0 V. It plateaus starting

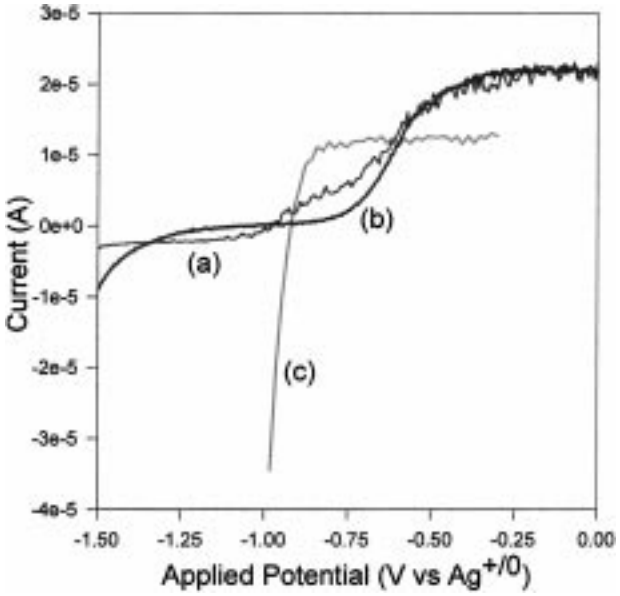

Figure 6. *I*−*V* curves for (a) laser-illuminated *n*-GaAs under the standard cell conditions described in the text, (b) laser-illuminated *n*-GaAs in a methanol cell containing no redox couple, and (c) ELH-lamp-illuminated *n*-GaAs under otherwise standard cell conditions.

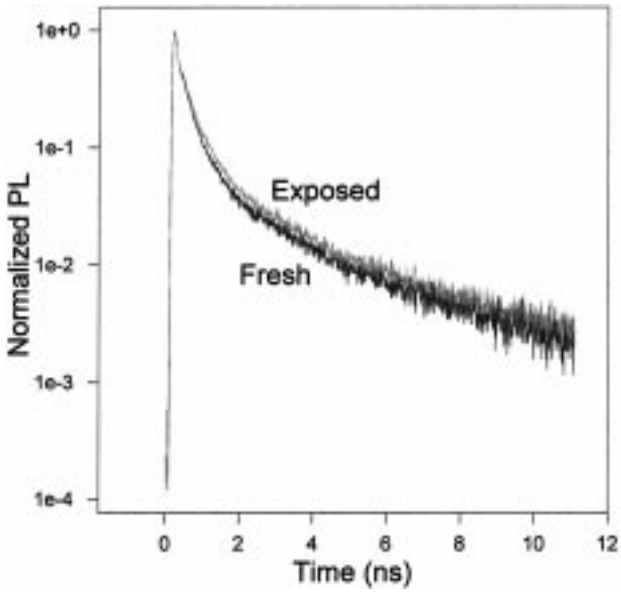

Figure 7. PL decays (951 kHz, 1.6×10^{13} photons/cm^2·pulse) taken at −0.9 V before and after exposure at −0.9 V vs $Ag^{+/0}$.

at −0.9 V, forming a small first peak, but then rises again at −0.7 V and plateaus starting at −0.5 V in a larger second peak. The redox couple in solution has a single one-electron oxidation/reduction so it can only be responsible for one oxidation peak. A plausible explanation for this behavior is that one of the peaks is from oxidation of the redox and the other is from corrosion of the cell. Three sets of experiments were performed to characterize these phenomena.

First, the optical experiments and electrochemistry were repeated on a cell without the redox couple present (Figure 6b). The *I*−*V* curve shows an oxidation peak during laser illumination in the same potential range as the second photocurrent peak (−0.7 to 0.0 V). This indicates that the redox couple is not responsible for both oxidation peaks.

Second, *I*−*V* curves were measured in cells that had the *n*-GaAs working electrode replaced with a platinum electrode (the RE in these cells was always $Ag/AgNO_3$). These *I*−*V* curves (not shown in the figures) do not show a second oxidation peak until the potential is beyond the stable potential window for methanol, greater than 1 V more positive than the redox equilibrium potential. Measuring the second oxidation peak (−0.7 to 0.0 V) requires the use of *n*-GaAs as the working electrode, which suggests that this peak is due to chemistry occurring on the *n*-GaAs surface. On the basis of these experiments, we conclude that the oxidation of the redox is assigned to the first oxidation peak (−0.9 to −0.7 V) and the corrosion process to the second oxidation peak (−0.7 to 0.0 V) in Figure 6a.

Finally, Figure 6c shows an *I*−*V* scan measured while the entire *n*-GaAs surface in contact with solution was illuminated with an ELH lamp (a well-known solar simulator).[27,28] This *I*−*V* curve shows only a single oxidation peak starting at −0.9 V. The second oxidation peak (starting at −0.7 V) is still present, but the light intensity is low enough that the redox couple is most likely already scavenging the majority of holes being produced. No increase in photocurrent is seen on moving into the potential region of the second oxidation peak because there are no additional holes available. Since the reaction rates are not well established for the two competing processes, it is uncertain which oxidation process predominates in scavenging the holes in this region.

Use of the ELH lamp was helpful in characterizing the photobehavior of the PEC in the low light intensity limit. *I*−*V* curves produced under ELH lamp illumination show a single oxidation peak that is stable over time for a cell that the picosecond laser system indicates is undergoing two independent oxidative processes. These experiments emphasize the usefulness of the laser system, which not only provides evidence of corrosion via the luminescence studies but also shows (in *I*−*V* curves) the potential window in which the corrosion occurs. An alternate method—which was not taken advantage of here but that other groups have used for overcoming this type of ambiguous *I*−*V* behavior—is the use of rotating ring disk voltammetry (RRDV) which can separate the corrosion current from the redox oxidation current.[29−31]

Figure 7 shows TRPL decays taken at −0.9 V, which is within the region of the first oxidation peak described above. It has already been shown that light exposure within the second oxidation peak (at 0.0 V; see Figure 2a,b) results in cell corrosion. To verify that the second peak (−0.7 to 0.0 V) corresponds to a corrosion process, it is important to differentiate its behavior from that of the first peak (−0.9 to −0.7 V). The decays taken before and after illumination at −0.9 V show no significant change in decay rate. We conclude that there is no corrosion occurring at this potential. The loss of the first peak in the absence of a redox couple and the lack of evidence of corrosion in the TRPL decays at −0.9 V support the assignment of the redox oxidation to the first peak and the corrosion process to the second peak.

The most likely source of corrosion in these cells is from residual water contamination. There are several models for the aqueous anodic corrosion of *n*-GaAs in the literature based on a variety of approaches including simple band diagrams,[32,33] Pourbaix diagrams,[34] kinetic models,[35,36] Tafel plots,[2,3] and RRDV.[29−31] Most relevant to the current study is the work by Vanmaekelbergh and Gomes[29] which includes mixed MeOH/H_2O corrosion studies on *n*-GaAs(111) and the work by Allongue and Blonkowski[2,3] which used the methanol/*n*-GaAs-(100) interface as a noncorroding reference for other corrosion work. In both cases *n*-GaAs is shown to be stable in acidic

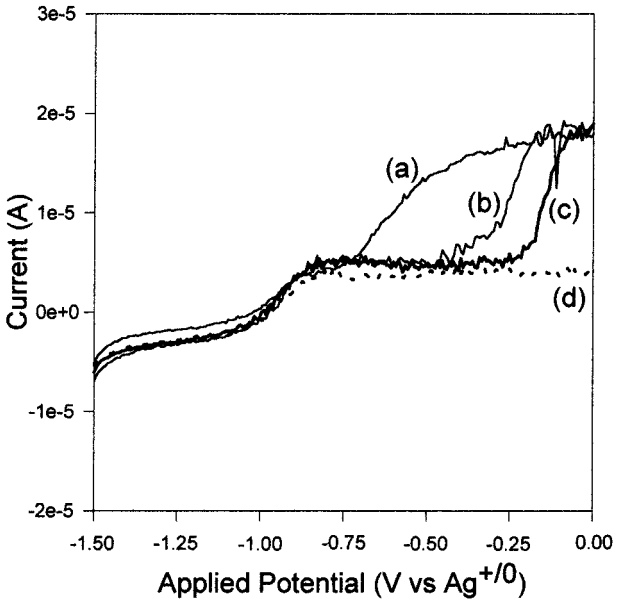

Figure 8. $I-V$ curves showing the effect of water addition to the cell: (a) no water added; (b and c) scans taken after 60−100 μL of water added; (d) >110 μL of water added.

methanol solutions. However, in the mixed methanol/water systems *n*-GaAs does corrode, albeit via a different proposed reaction mechanism than for strictly aqueous systems. The current study was performed in a regime where methanol is not oxidized (as indicated by stable *I-V* curves with a platinum WE), ruling out methanol oxidation as a component in the corrosion process. The reported stability of *n*-GaAs in methanol and the notorious difficulty in keeping methanol dry[37] in experiments performed outside of a drybox are sufficient evidence to suggest water is the most likely cause of the corrosion observed in this study.

D. Incremental Water Addition. To help determine the effects of water contamination on the PEC, a series of water additions were made with the PL and $I-V$ behavior being monitored between each addition. Representative $I-V$ results are presented in Figure 8. All of the $I-V$ scans were taken with a 20 mV/s scan rate. Ten μL at a time was added to a cell containing 50 mL of methanol (plus redox and inert electrolyte). Three distinct behavioral regions were observed in the cells, depending on total water content. First, with less than 60 μL of H_2O added the $I-V$ curves look the same as an uncontaminated PEC (Figure 8a). Second, when a total of 60−100 μL is added, a portion of the photocurrent is lost while sweeping into reverse bias (Figure 8b,c), but reappears on the return sweep toward forward bias (not shown in the figure). If shown, the return sweep toward forward bias would follow the current path of the uncontaminated cell (Figure 8a). A larger potential range is lost on the sweep into reverse bias with each 10 μL water addition. Figure 8c has more water added than Figure 8b. It appears that, in this range, some process is inhibiting the passage of current until it is overcome by a strong enough anodic (reverse bias) potential. Once overcome, the inhibiting process is not renewed until the potential is swept back into forward bias. Third, with greater than 110 μL added, there is a significant loss in photocurrent (Figure 8d), showing the same $I-V$ behavior as found in Figure 5 (iii). The loss in photocurrent extends to the most positive potential, applied to the cell. This loss is not overcome by the applied reverse bias potential and the photocurrent stays small even on the return sweep toward forward bias.

The degradation of the PL−V behavior at all potential ranges (Figure 4a (iii)) and the gradual loss of the oxidation peak in the $I-V$ scans (Figure 8) support the idea of a buildup of an oxidation layer pinning the fermi level of the *n*-GaAs and interfering with charge-transfer processes. With low water contamination, the oxide layer incompletely passivates the surface and can be overcome electrochemically. A component of this film may arise from the decomposition of ferricenium, which is known to cause electrode fouling in electrochemical studies involving acetonitrile.[38]

IV. Conclusions

At the light intensities employed in this study, the intrinsic surface states of the *n*-GaAs/methanol interface are saturated, making it a viable system for the examination of photoinduced surface states. Similar to the aqueous cells studied previously in this lab, these cells corrode anodically, resulting in the creation of surface states within the *n*-GaAs band gap. The drop in PL and increase in the TRPL decay rate at all measured potentials show a distribution of PSS across the band gap. However, the corrosion only occurs when the cell is held in the potential range corresponding to the second oxidation peak in the $I-V$ curves (−0.7 to 0.0 V). Exposure of the cell to light while maintaining a potential in the first oxidation peak (−0.9 to −0.7 V) does not result in cell corrosion. By careful choice of the potential range in which experiments are performed, we are able to use cell corrosion as a controllable parameter in studying the *n*-GaAs/methanol interface. We attribute the photocorrosion in the cell to trace amounts of residual water in the electrolyte.

This investigation has illuminated several important differences in the behavior of corroded methanol cells from the behavior of corroded aqueous cells. First, repetition rate studies indicate that the lifetime of hole trapping in PSS in the methanol cells is longer than the 4 μs maximum lifetime determined for the aqueous cells. Second, unlike the PSS in the aqueous work, the PSS in methanol are not charge-transfer inhibitors. The photocurrent does not decrease with cell corrosion. Third, despite the low concentration of the redox couple in the methanol cells, the corrosion results in a distribution of PSS similar to that in corroded high-concentration Na_2S aqueous cells.

Small amounts of water have profound effects on the characteristics of the *n*-GaAs(100)/methanol interface. The cell appears to have some ability to withstand or compensate for water contamination, as a small water addition (up to 60 μL in a 50 mL cell) does not appear to affect the PL−V profile or the photocurrent. However, after enough water is added (>60 μL), both the photocurrent and photoluminescence are reduced dramatically. These effects are attributed to the buildup of an oxide/adsorbate layer on the surface of the semiconductor. This can account for both the decrease in current and the loss of the voltage dependence of the photoluminescence.

Future work is planned to elucidate more information about the cause of the corrosion and the cell parameters that affect the corrosion such as voltage scan rate, redox concentration, water concentration, and light intensity at the interface.

Acknowledgment. We gratefully acknowledge the financial support of the Department of Energy, Basic Energy Sciences (Grant DE-FG06-86ER45273).

References and Notes

(1) Tan, M. X.; Laibinis, P. E.; Nguyen, S. T.; Kesselman, J. M.; Stanton, C. E.; Lewis, N. S. Principles and Applications of Semiconductor

Photoelectrochemistry. In *Progress in Inorganic Chemistry*; Karlin, K. D., Ed.; John Wiley & Sons: New York, 1994; Vol. 41, pp 21−144.
(2) Allongue, P.; Blonkowski, S. *J. Electroanal. Chem.* **1991**, *316*, 57−77.
(3) Allongue, P.; Blonkowski, S. *J. Electroanal. Chem.* **1991**, *317*, 77−99.
(4) Lingier, S.; Gomes, W. P.; Cardon, F. *Ber. Bunsen-Ges. Phys. Chem.* **1989**, *93*, 2−7.
(5) Ba, B.; Fotouhi, B.; Gabouze, N.; Gorochov, O.; Cachet, H. *J. Electroanal. Chem.* **1992**, *334*, 263−277.
(6) Lunt, S. R.; Ryba, G. N.; Santangelo, P. G.; Lewis, N. S. *J. Appl. Phys.* **1991**, *70*, 7449−7467.
(7) Lunt, S.; Santangelo, P. G.; Lewis, N. S. *J. Vac. Sci. Technol., B* **1991**, *9*, 2333−2336.
(8) Rosenwaks, Y.; Thacker, B. R.; Ahrenkiel, R. K.; Nozik, A. J. *J. Phys. Chem.* **1992**, *96*, 10096−10098.
(9) Bessolov, V. N.; Konenkova, E. V.; Lebedev, M. V. *J. Vac. Sci. Technol., B* **1996**, *14*, 2761−2766.
(10) Bessolov, V. N.; Lebedev, M. V.; Binh, N. M.; Friedrich, M.; Zahn, D. R. T. *Semicond. Sci. Technol.* **1998**, *13*, 611−614.
(11) Balko, B. A.; Richmond, G. L. *J. Phys. Chem.* **1993**, *97*, 9002−9008.
(12) Pleskov, Y. V.; Gurevich, Y. Y. *Semiconductor Photoelectrochemistry*; Consultants Bureau: New York, 1986.
(13) Morrison, S. R. *Electrochemistry at Semiconductor and Oxidized Metal Electrodes*; Plenum Press: New York, 1980.
(14) Kauffman, J. F.; Balko, B. A.; Richmond, G. L. *J. Phys. Chem.* **1992**, *96*, 6371−6374.
(15) Kauffman, J. F.; Balko, B. A.; Richmond, G. L. *J. Phys. Chem.* **1992**, *96*, 6374−6377.
(16) Ellis, A. B.; Bolts, J. M.; Kaiser, S. W.; Wrighton, M. S. *J. Am. Chem. Soc.* **1977**, *99*, 9−15.
(17) Balko, B. A.; Miller, E. A.; Richmond, G. L. *J. Phys. Chem.* **1995**, *99*, 4124−4131.
(18) Miller, E. A.; Richmond, G. L. *J. Phys. Chem. B* **1997**, *101*, 2669−2677.
(19) O'Connor, D. V.; Phillips, D. *Time-Correlated Single Photon Counting*; Academic Press: London, 1984.
(20) Yariv, A. *Optical Electronics*; Holt, Rinehart, & Winston: New York, 1986.
(21) Palik, E. D. *Handbook of Optical Constants of Solids*; Academic Press: Orlando, FL, 1985.
(22) Archer, M. D.; Bolton, J. R. *J. Phys. Chem.* **1990**, *94*, 8028.
(23) Orton, J. W.; Blood, P. *The Electrical Characterization of Semiconductors: Measurement of Minority Carrier Properties*; Academic Press: London, 1990.
(24) Kauffman, J. F.; Richmond, G. L. *J. Appl. Phys.* **1993**, *73*, 1912−1917.
(25) Kauffman, J. F.; Richmond, G. L. *Appl. Phys. Lett.* **1991**, *59*, 561−563.
(26) Nozik, A. J. *Annu. Rev. Phys. Chem.* **1978**, *29*, 189−222.
(27) Gronet, C. M.; Lewis, N. S. *J. Phys. Chem.* **1984**, *88*, 1310−1317.
(28) Tan, M. X.; Newcomb, C.; Kumar, A.; Lunt, S. R.; Sailor, M. J.; Tufts, B. J.; Lewis, N. S. *J. Phys. Chem.* **1991**, *95*, 10133−10142.
(29) Vanmaekelbergh, D.; Gomes, W. P. *J. Phys. Chem.* **1990**, *94*, 1571−1575.
(30) Lingier, S.; Vanmaekelbergh, D.; Gomes, W. P. *J. Electroanal. Chem.* **1987**, *228*, 77−88.
(31) Memming, R. *J. Electrochem. Soc.* **1978**, *125*, 117−123.
(32) Gerischer, H. *J. Electroanal. Chem.* **1977**, *82*, 133−143.
(33) Bard, A. J.; Wrighton, M. S. *J. Electrochem. Soc.* **1977**, *124*, 1706−1710.
(34) Park, S.-M.; Barber, M. E. *J. Electroanal. Chem.* **1979**, *99*, 67−75.
(35) Jr., K. W. F.; Madou, M. J.; Morrison, S. R. *J. Phys. Chem.* **1980**, *84*, 3172−3178.
(36) Jr., K. W. F.; Madou, M. J.; Morrison, S. R. *J. Electrochem. Soc.* **1981**, *128*, 1527−1531.
(37) Rosa-Montañez, M. E.; Jesús-Cardona, H. D.; Cabrera, C. R. *Electrochim. Acta* **1997**, *42*, 1839−1846.
(38) Zotti, G.; Schiavon, G.; Zecchin, S.; Favretto, D. *J. Electroanal. Chem.* **1998**, *456*, 217−221.